Bifurcation analysis of nonlinear reaction-diffusion problems using wavelet-based reduction techniques

J. Krishnan[1, *] O. Runborg[2, †]
I. G. Kevrekidis[1, 2]

[1] Department of Chemical Engineering;
[2] Program in Applied and Computational Mathematics
Princeton University, Princeton, NJ 08544.

August 26, 2003

Abstract

Using a computational method for numerical homogenization, we perform the coarse-scale bifurcation analysis of nonlinear reaction-diffusion problems in both uniform and spatially varying media. The method is based on wavelet decomposition and projection of the differential equation on coarse scale wavelet spaces. The approach is capable of capturing turning points and pitchfork bifurcations of sharp, front-like solutions at the coarse level.

Key words: wavelets, numerical homogenization, bifurcation analysis, reaction-diffusion equations

1 Introduction

Physical systems with multiple length and/or time scales are routinely encountered in science and engineering. Since it is computationally too expensive to describe all scales of a physical system in detail, incorporating the full range of phenomena involved, coarse-graining approximations have to be made at various stages. The most common of these is the continuum approximation, averaging over atomic scale effects, yielding partial differential equation descriptions of the field variables describing the problem.

*Current address: Dept. of Electrical Eng., Johns Hopkins University 105 Barton Hall, 3400 N. Charles St., Baltimore MD 21218.

† *To whom correspondence should be addressed.* Current address: NADA, KTH, 100 44 Stockholm, Sweden. Email: `olofr@nada.kth.se`

In some cases, the effect of physics at small scales on the behavior at the macro-scale (the scale of interest) can be incorporated through phenomenological coefficients (fluid viscosities, effective permeabilities) which can be obtained through experiments or microscopic simulations. For example in a macroscopic description of a complex fluid, molecular dynamics can be used to obtain transport coefficients, which are then used in a macroscopic model, see [4].

Even in continuum problems, however, phenomena may occur over a range of scales, as in the case of a fine-grained composite material or of transport in porous media. A full numerical simulation of such models in the form of differential equations with rapidly varying coefficients is usually computationally prohibitive, since the small scale variations need to be resolved. An accurate reduced model, describing the system at the scale of interest would therefore be of enormous practical importance.

One of the classical analytical approaches to obtaining such reduced models is *homogenization*, [5, 20]. There a simplified, "homogenized" or "effective", equation is derived, whose solution represents the coarse scale part of the full solution. If, for example, the profile of the relevant field variable (temperature in heat transfer problems, concentration in diffusion problems) is in the form of small variations about a smooth envelope, the effective equation would describe the smooth envelope. The effective equation is typically less expensive to solve numerically, since the small scales are already averaged out.

Homogenization can be used for some classes of problems, such as linear elliptic equations with periodic or certain types of stochastic coefficients. It has also been applied to problems in linear wave propagation—for example acoustic wave propagation in disordered media, and elastic wave propagation in heterogeneous composites—and problems involving composite materials, for example, material properties of fiber reinforced composites, and transport in heterogeneous and porous media, like groundwater transport in soil, or transport in rock.

When applicable, homogenization is truly valuable. In practical problems, however, its application is restricted mainly by two factors: the assumption of a special structure on the coefficients and equations, and the assumption of a clear separation of length scales. Neither assumption may hold in many practical cases: porous media may have several length scales with no clear separation and their pore structure is not periodic. For complicated problems, including most nonlinear equations, no simple way to express the effective equation is available, and, for that matter, an effective equation may not exist.

An alternative approach to derive effective equations for problems with multiscale structure is a wavelet based, numerical approach, pioneered by Beylkin and Brewster [6]. The method uses multiresolution analysis and wavelet decompositions of the differential equation to derive compact coarse scale models. It involves systematically taking into account effects on the fine-scale wavelet spaces and projecting them onto coarser scales, achieving a "transfer" from finer to coarser scale of the detailed governing equation. The numerical algorithm thus computes a modified differential equation on the coarser scale, whose solution is the coarse scale component of the "fine" solution (i.e. the full solution on the finer scale). This procedure is repeated hierarchically until one reaches the scale of interest. The approach systematically takes the microstructure into account, and obtains the equation at the coarse scale without any assumptions on its structure (functional form).

When the equations are linear, a straightforward way of performing this reduction and representing the effective equation exists. It has been studied in [6, 10, 1, 8, 14, 28, 32] for various equations and settings, see also [11]. The method was extended to a class of nonlinear problems by Gilbert, Beylkin and Brewster [7]. In this case there is in general no closed form representation for the effective equation. Instead, one either needs to represent it numerically on a grid, or use a closed form approximate representation based on Taylor expansions.

Another application of a (quite different) wavelet-based approach was considered in [24, 30]. Here the problem was one of transport via conduction in a highly disordered two-dimensional medium. The medium was represented by a two-dimensional conductance network, which contains the morphological information. In this case, wavelets were used to determine the level of contrast between the conductances at adjacent bonds. If the contrast was small (i.e. smaller than a certain pre-fixed threshold), the adjacent nodes were regarded as one (i.e. the bond connecting them can be removed). By performing such an operation over a few scales, a fairly significant reduction in the number of equations and unknowns was possible.

Other numerical approaches to the homogenization problem also exist in the literature, such as coarsening techniques from algebraic multigrid, see e.g. Knapek [21], Neuss et al [27] and Moulton et al. [25], as well as multiscale finite element methods, see e.g. Hou et al. [17, 18], Hughes [19], Babuška [2], Matache and Schwab [23]. We have recently proposed a "coarse timestepper" based method [29].

In this paper we discuss the application of the wavelet-based reduction techniques in [7, 15, 13], employing the Taylor expansion approximation, to nonlinear boundary value problems arising in the study of steady states of reaction-diffusion systems. Nonlinear reaction-diffusion systems occur widely as models of pattern formation in chemical and biological media. Even when the media are homogeneous, patterns with nontrivial spatial structure (pulses, fronts, spiral waves, target patterns) can spontaneously emerge. We are particularly interested in heterogeneous media, in which the heterogeneity can exert a strong influence on the patterns formed. This interest has developed through our research on microcomposite catalysts [16, 3, 22], where microlithography is used to decorate the surface of a metal catalyst (usually Pt) with a pattern of heterogeneities, consisting of different catalytic materials (e.g. Rh, Pd, or even inactive Ti). The illustrative model in this paper will be the FitzHugh-Nagumo (FHN) system of PDEs [12, 26], which have been derived in the context of neurophysiology. Depending on parameter values, these are capable of generating the same qualitative types of patterns as the more complicated mechanistic models of the catalytic reactions (like the oxidation of CO) that we study on microcomposite catalysts. The FHN equations will be studied using the reduction approach with both uniform and spatially varying coefficients (simulating uniform and spatially varying reactive media).

Our goal is to obtain the reduced equations for such systems and evaluate their ability to capture the behavior at a coarse level. In particular, we will focus on the ability of coarse models to capture the bifurcation behavior of the underlying detailed problem. We will study bifurcations due to variation of the macroscopic system parameters, as well as due to variations in the "microstructure": the amplitude and wavelength of the variations in the medium. That the "detailed model" parameters enter transparently in the coarse equations derived is, we believe, a strong point of the procedure.

The paper is structured as follows: Section 2 briefly discusses the wavelet-based reduction techniques for linear problems as introduced by Beylkin and Brewster. Section 3 discusses the extension of this technique to nonlinear problems. Section 4 describes the reduction of the FHN system both in the nondiffusing inhibitor case (resulting in a scalar Boundary Value Problem, BVP) and in the diffusing inhibitor case (resulting in a BVP system). Section 5 contains our computational results, including fine and coarse bifuraction diagrams and convergence studies. We conclude in Section 6. A brief summary of useful facts about wavelets is presented in an appendix.

2 Wavelet-based reduction techniques for linear problems

Here we briefly review the wavelet-based numerical homogenization for systems governed by linear differential equations. Without going into all the details of the calculations, we will focus on the main methodology involved. For more details, the reader is referred to [6].

The implementational aspects of the algorithms under consideration use wavelets in a rather simple way, relying on the basic Haar wavelet. All the problems in this paper will be formulated on the unit interval, after rescaling of the domain. All the functions under consideration will be square integrable on this domain. We let V_n and W_n denote the usual scaling and wavelet spaces of the Haar system. They satisfy

$$V_n \subset V_{n+1}, \qquad V_n \oplus W_n = V_{n+1}, \qquad V_n \perp W_n.$$

The space V_n is the space of functions on the next coarser scale with respect to V_{n+1}, and W_n is the component of V_{n+1} which contains the fine scale information. The index $n \geq 0$ indicates the level of coarseness (scale), with 0 corresponding to the coarsest. In the Haar case, V_n and W_n contain piecewise constant functions. More background about wavelets and terminology can be found in Appendix A.

We emphasize again that the main difficulty arises because of the multiscale nature of the differential equations, even if they are linear. Since a hierarchy of scales is naturally defined in the wavelet basis, the main step in the algorithm is the transfer, from a fine scale to the next coarser scale, of the equation and the solution to the equation at that scale (without directly computing this solution). If the equation is written in a suitable operator form, the transfer from one scale to the next coarser scale preserves the form of the equation. This means that the process can be applied recursively until the scale of interest is reached, at which point the resulting equation is directly solved.

Let us for simplicity start out with a scalar equation (the vector case is treated analogously) of the form

$$\begin{aligned} \frac{dy}{dx} &= Fy, \\ y(0) &= y_0. \end{aligned}$$

In general F is a linear operator which may depend on x in a complicated way. Integrating both sides from 0 to x gives,

$$y(x) - y_0 = \int_0^x F(s)y(s)ds.$$

We will consider a more general equation

$$G(x)y(x) - y_0 = \int_0^x F(s)y(s)ds,$$

where also $G(x)$ is a linear operator. Letting K denote the integration operator, this can be written as

$$Gy - y_0 = KFy.$$

We now discretize this equation by replacing the operators G, K and F with their projections on the fine scale space V_n for some large n (to reasonably capture all the fine scale property variations in the equations),

$$G_n y_n - y_0 = K_n F_n y_n. \tag{1}$$

Denoting the projection operator onto the space V_n by P_n, the components in the discretized equation is thus given by

$$G_n = P_n G P_n, \qquad F_n = P_n F P_n, \qquad K_n = P_n K P_n, \tag{2}$$

and the new unknown y_n is an approximation of $P_n y$. We should observe here that the V_n and W_n spaces are finite dimensional, more precisely of dimension 2^n. Functions belonging to them can therefore be identified by vectors in $\mathbb{R}^{2^n}$, where the entries are coefficients for the bases (see (14) and (15) in the Appendix). In the Haar case, those entries are simply the piecewise constant values of the function, scaled by $2^{n/2}$. Operators acting on the functions can similarly be represented by matrices, and (1) is really a linear system of equations, where the unknown y_n is a vector with 2^n components and G_n, K_n, F_n are $2^n \times 2^n$ matrices. At this stage, we simply have the discretized form of the full equation, which we want to avoid solving directly.

The essence of the algorithm is to organize the "transfer" of equation (1) and the corresponding solution from scale to scale. To do this the solution is first split into its components in the coarse (belonging to V_{n-1}) and fine (belonging to W_{n-1}) scales,

$$y_n = P_{n-1}y_n + Q_{n-1}y_n =: v_{n-1} + w_{n-1}, \qquad v_{n-1} \in V_{n-1}, \quad w_{n-1} \in W_{n-1}.$$

Here Q_{n-1} is the projection operator onto the subspace W_{n-1}, which contains information about the difference (contrast) between values at every successive pair of intervals. In the Haar case v_{n-1} corresponds to simply taking the sum of the elements of y_n at every successive pair of intervals (at scale n), and w_{n-1} to the difference between elements of y_n (an illustration is shown in Appendix A).

We now also split the equation by applying the projection operators P_{n-1} and Q_{n-1}. The application of P_{n-1} to (1) results in

$$\begin{aligned} &P_{n-1}G_nP_{n-1}v_{n-1} + P_{n-1}G_nQ_{n-1}w_{n-1} - y_0 \\ &\qquad = \quad P_{n-1}K_nF_nP_{n-1}v_{n-1} + P_{n-1}K_nF_nQ_{n-1}w_{n-1}. \end{aligned} \tag{3}$$

This is the equation on the coarse scale. The terms containing w_{n-1} represent fine scale information. Disregarding those would mean that the fine scale information is not "passed onto" the coarse scale. Projecting (1) also onto W_{n-1} (applying Q_{n-1} to it) gives

$$\begin{aligned} &Q_{n-1}G_nP_{n-1}v_{n-1} + Q_{n-1}G_nQ_{n-1}w_{n-1} \\ &\qquad = \quad Q_{n-1}K_nF_nP_{n-1}v_{n-1} + Q_{n-1}K_nF_nQ_{n-1}w_{n-1}. \end{aligned}$$

This is a linear equation which can be solved for w_{n-1} in terms of v_{n-1}. When the result is plugged back into (3) we have a *closed* equation on the coarse scale *involving only coarse scale quantities.* This equation turns out to be of the form

$$G_{n-1}v_{n-1} - y_0 = K_{n-1}F_{n-1}v_{n-1}.$$

Here K_{n-1} is defined as before, $K_{n-1} = P_{n-1}KP_{n-1}$, while G_{n-1} and F_{n-1} are given by formulae involving only G_n, F_n and K_n. Note that this equation has the same form as (1), the equation on the previous scale, with $v_{n-1} = P_{n-1}y_n$ taking the role of y_n. The left hand side is the product of a matrix and the vector corresponding to the function at that scale, from which is subtracted the initial condition. The right hand side is the action of the integral operator for that scale on the product of a matrix and the vector corresponding to the function at that scale. The initial condition is unaffected by this reduction procedure, and can be regarded as a parameter for the reduction process. Also notice that, when represented as vectors and matrices, the variables are half the size compared with the starting equation. Thus one step in the reduction procedure has led to a linear system of reduced size involving only the coarse scale quantities at scale $n-1$.

Since the form of the equation is preserved upon reduction, and the various matrices (operators) at a given scale can be obtained in terms of matrices at the previous (finer) scale the process can be iterated until we reach the scale of interest. In particular if we reduce all the way to the end (i.e., the scale $n = 0$), we get a simple scalar linear equation for the average of the solution over the entire domain (which is the coarse scale component of the full solution at scale $n = 0$). Thus, if we are only interested in the average of the solution over the entire domain, all we have to do is solve the reduced (scalar linear) equation at scale $n = 0$, rather than solve the full equation and then compute the average of the detailed solution.

3 Reduction for nonlinear systems

In the nonlinear case the formal approach for equation reduction is very similar to the linear case. The main difference comes in implementing the recurrence relations. The projection operation does not split the equations into separate terms, containing coarse and fine scale information; here they are coupled. The ease of elimination in the linear case is, in principle, lost.

Consider a single nonlinear ODE

$$\begin{aligned} \frac{dy}{dx} &= f(x,y), \\ y(0) &= y_0. \end{aligned}$$

This can again be written in the form of an integral equation. We consider the slightly more general integral equation

$$G(x, y(x)) - y(0) = \int_0^x F(s, y(s))ds.$$

We discretize this in analogy with (1,2),

$$G_n(y_n) - y_0 = K_n F_n(y_n), \tag{4}$$

where $y_n \approx P_n y$ and

$$G_n(y(x)) = P_n G(x, P_n y), \qquad F_n(y(x)) = P_n F(x, P_n y), \qquad K_n = P_n K P_n. \tag{5}$$

In order to express this as a finite dimensional problem we will use almost the same Haar basis functions as in the linear case, but since G and F are now nonlinear functions, it will be more convenient to rescale the V_n basis functions (14) by $2^{-n/2}$ and the W_n basis functions (15) by $2^{n/2}$. Now $v_n(x) \in V_n$ is identified with the vector $\tilde{v}_n \in \mathbb{R}^{2^n}$ whose elements are the piecewise constant values of $v_n(x)$. A function $w_n \in W_n$, on the other hand, is identified with a vector $\tilde{w}_n \in \mathbb{R}^{2^n}$ whose elements are the divided differences of the piecewise constant values of $w_n(x)$. In what follows we will drop the tilde in the notation and use $y_n(k)$ to denote the k-th element of the vector y_n.

The finite dimensional problem can then be written as

$$y_n \in \mathbb{R}^{2^n}, \qquad y_n(k) \approx \frac{1}{\delta_n} \int_{k\delta_n}^{(k+1)\delta_n} y(x)dx, \qquad \delta_n = 2^{-n},$$

$$G_n(y_n) \in \mathbb{R}^{2^n}, \qquad G_n(y_n)(k) = g_n(k, y_n(k)) := \frac{1}{\delta_n} \int_{k\delta_n}^{(k+1)\delta_n} G(x, y_n(k))dx,$$

and similarly for $F_n(y_n) \in \mathbb{R}^{2^n}$, $F_n(y_n)(k) = f_n(k, y_n(k))$. Finally,

$$K_n = \delta_n \begin{pmatrix} \frac{1}{2} & 0 & \dots & 0 \\ 1 & \ddots & \ddots & \vdots \\ \vdots & \ddots & \ddots & 0 \\ 1 & \dots & 1 & \frac{1}{2} \end{pmatrix} \in \mathbb{R}^{2^n \times 2^n},$$

and $y_0 \in \mathbb{R}^{2^n}$ is a constant vector.

The above is simply the discretized version of the full problem, with all variables (and functions) represented as piecewise constant entities on a grid of size 2^n. Note that the explicit dependence of the functions F and G on the spatial variable has been averaged out in each of the 2^n "subdomains", as seen above.

The first main result of the nonlinear reduction procedure developed in [7] states that a reduction of the fine scale equation (4) to the next coarser scale can be accomplished in a way similar to the linear case. By projecting it on both the fine and coarse scales, the fine scale part of the solution can be eliminated, leaving an equation only for the coarse scale part. In order to pass to the next scale, we thus introduce the projection operators, which in the rescaled Haar basis will be denoted $S_{n-1} : V_n \mapsto V_{n-1}$ and $D_{n-1} : V_n \mapsto W_{n-1}$. They are defined as

$$\begin{aligned} S_{n-1}y_n = s_{n-1} \in \mathbb{R}^{2^{n-1}}, \qquad s_{n-1}(k) &= \frac{1}{2}(y_n(2k+1) + y_n(2k)), \\ D_{n-1}y_n = d_{n-1} \in \mathbb{R}^{2^{n-1}}, \qquad d_{n-1}(k) &= \frac{1}{\delta_n}(y_n(2k+1) - y_n(2k)). \end{aligned}$$

In the above equations, the operator S_{n-1} acting on a vector, produces a vector of half the size, with each component being the average of the corresponding pair in the original vector. The operator D_{n-1} acting on a vector, produces a vector of half the size, with each component being the scaled difference of the corresponding pair in the original vector. Clearly the operators S_{n-1} and D_{n-1} produce the coarse scale and fine scale components of a vector. Applying the operators S_{n-1} and D_{n-1} to (4) gives

$$\begin{aligned} S_{n-1}G_n(y_n) - y_0 &= S_{n-1}K_nF_n(y_n), \\ D_{n-1}G_n(y_n) &= D_{n-1}K_nF_n(y_n), \end{aligned}$$

and after using the easily verifiable formulae,

$$D_{n-1}K_n = S_{n-1}, \qquad S_{n-1}K_n = K_{n-1}S_{n-1} - \frac{\delta_n^2}{4}D_{n-1},$$

they become

$$\begin{aligned} S_{n-1}G_n(y_n) - y_0 &= K_{n-1}S_{n-1}F_n(y_n) - \frac{\delta_n^2}{4}D_{n-1}F_n(y_n), && (6) \\ D_{n-1}G_n(y_n) &= S_{n-1}F_n(y_n). && (7) \end{aligned}$$

We note that

$$\begin{aligned}
S_{n-1}G_n(y_n)(k) &= \frac{1}{2}\left[g_n\left(2k+1, y_n(2k+1)\right) + g_n(2k, y_n(2k))\right] \\
&= \frac{1}{2}\left[g_n\left(2k+1, s_{n-1}(k) + \frac{\delta_n}{2}d_{n-1}(k)\right)\right. \\
&\quad \left. + g_n\left(2k, s_{n-1}(k) - \frac{\delta_n}{2}d_{n-1}(k)\right)\right] \\
&=: Sg_n(k, s_{n-1}(k), d_{n-1}(k)), \qquad (8)
\end{aligned}$$

and similarly for Dg_n, Sf_n and Df_n. In the above equation, the first argument for the function g_n denotes its explicit spatial dependence, and the others denote its dependence on the variable y_n, which of course also has a spatial variation.

Then (7) can be solved for each component k in order to get $d_{n-1}(k)$ as a function of $s_{n-1}(k)$. The nonlinear equation (7) is assumed to (at least locally) define a function h_{n-1} such that

$$Dg_n(k, s_{n-1}(k), h_{n-1}(k, s_{n-1}(k))) = Sf_n(k, s_{n-1}(k), h_{n-1}(k, s_{n-1}(k))),$$

for each k. This is used to eliminate the fine scale part of y_n from (6,7). The reduced equation on level $n-1$ then follows from (6),

$$G_{n-1}(s_{n-1}) - y_0 = K_{n-1}F_{n-1}(s_{n-1}),$$

where

$$\begin{aligned}
G_{n-1}(s_{n-1})(k) &= g_{n-1}(k, s_{n-1}(k)) := Sg_n(k, s_{n-1}(k), h_{n-1}(k, s_{n-1}(k))) \\
&\quad + \frac{\delta_n^2}{4}Df_n(k, s_{n-1}(k), h_{n-1}(k, s_{n-1}(k))).
\end{aligned}$$

$$F_{n-1}(s_{n-1})(k) = f_{n-1}(k, s_{n-1}(k)) := Sf_n(k, s_{n-1}(k), h_{n-1}(k, s_{n-1}(k))).$$

Thus, when the equation is written in integral form, and then discretized, elimination still preserves its form. As in the linear case, the procedure can be repeated recursively till we arrive at the coarseness level of interest.

While the above derivation is formally clear, it is not very practical for implementing a recursion relation, since the equation (7) which determines d_{n-1} is nonlinear. Beylkin *et al.* [7] suggested performing a Taylor series expansion in δ_n of (6,7) to circumvent this problem. For instance, since

$$\begin{aligned}
Dg_n(k, s, d) &= Dg_n(k, s, 0) + dSg_n'(k, s, 0) + O(\delta_n^2), \\
Sf_n(k, s, d) &= Sf_n(k, s, 0) + O(\delta_n^2),
\end{aligned}$$

we have

$$d_{n-1}(k) = \frac{Sf_n(k, s_{n-1}(k), 0) - Dg_n(k, s, 0)}{Sg_n'(k, s_{n-1}(k), 0)} + O(\delta_n^2).$$

Here Sg'_n is defined as

$$Sg'_n(k, s_{n-1}(k), d_{n-1}(k)) := \frac{1}{2}\left[\frac{\partial g_n}{\partial y}(2k+1, y_n(2k+1)) + \frac{\partial g_n}{\partial y}(2k, y_n(2k))\right].$$

More generally assume that at some scale j we can write the functions $g_j(k, s)$ and $f_j(k, s)$ as a sum of two terms one of $O(1)$ and one of $O(\delta_j^2)$ as

$$\begin{aligned} g_j(k,s) &= \gamma_{0,j}(k,s) + \gamma_{1,j}(k,s)\delta_j^2, \\ f_j(k,s) &= \theta_{0,j}(k,s) + \theta_{1,j}(k,s)\delta_j^2. \end{aligned}$$

This is just motivated by the Taylor series approximation. The functions $\gamma_{0,j}$ and $\gamma_{1,j}$ can be thought of two "pieces" of the function g_j, and similarly for f_j. We may then perform the reduction of this equation to a similar one at scale $j-1$, where

$$\begin{aligned} g_{j-1}(k,s) &= \gamma_{0,j-1}(k,s) + \gamma_{1,j-1}(k,s)\delta_{j-1}^2, \\ f_{j-1}(k,s) &= \theta_{0,j-1}(k,s) + \theta_{1,j-1}(k,s)\delta_{j-1}^2. \end{aligned}$$

The recursion relations for the functions f_j and g_j, which enable their determination at every successive scale, can now be written as recursion relations involving the functions $\gamma_{0,j}$, $\gamma_{1,j}$, $\theta_{0,j}$, $\theta_{1,j}$. In succint form they are

$$\begin{aligned} \gamma_{0,j-1} &= S\gamma_{0,j}, \\ \theta_{0,j-1} &= S\theta_{0,j}, \\ \gamma_{1,j-1} &= \frac{1}{4}S\gamma_{1,j} + \frac{d_{j-1}}{16}(D\gamma'_{0,j} + S\gamma'_{0,j}) + \frac{1}{16}D\theta_{0,j} + \frac{d_j^2}{32}S\gamma''_{0,j}, \\ \theta_{1,j-1} &= \frac{1}{4}S\theta_{1,j} + \frac{d_{j-1}}{16}D\theta'_{0,j-1} + \frac{d_{j-1}^2}{32}S\theta''_{0,j}, \\ d_{j-1} &= \frac{S\theta_{0,j} - D\gamma_{0,j}}{S\gamma'_{0,j}}, \end{aligned} \tag{9}$$

where the functions on the right hand side are evaluated with the last argument ($d_{j-1}(k)$) equal to zero (see above).

The functions f_j and g_j can thus be arranged so as to contain two terms of appropriate orders, and recursion relations can be written for each of those terms. The functions $\gamma_{0,n}$ and $\theta_{0,n}$ (as functions of the dependent variable, and possibly any spatially dependent parameter in the equation) at scale n are determined from the differential equation; the functions $\gamma_{1,n}$ and $\theta_{1,n}$ are set to zero. Thereafter, these functions at any scale are determined recursively from their values at the previous scale, using (9); they are determined as combinations of terms involving the application of the operators S and D on the same functions at scale j. In particular, we can perform a reduction all the way to the coarsest scale ($j = 0$) such that $\theta_{0,0}$, $\theta_{1,0}$, $\gamma_{0,0}$, $\gamma_{1,0}$ are all non-linear functions of the solution average over the whole interval (which is the component of the solution on the coarsest scale). The reduced equation at the coarsest scale is a single nonlinear algebraic equation which can be solved to obtain an approximation to this solution average. Note that the approximation introduced in this result comes from truncating Taylor series at each level.

To summarize, in this subsection, we have described how the reduction procedure for a single, non-linear differential equation can be performed. While conceptually similar to the linear case, the important difference is that the solution of a non-linear equation is required to determine the variable d_{n-1} and pass on the relevant information to the coarser scale. This was accomplished by a Taylor series approximation.

3.1 Systems of equations

The procedure described above can be extended in a straightforward way to apply to systems of differential equations; the corresponding Taylor series are now multivariate.

Suppose we have a system of first order ODEs (initial value problem),

$$\begin{aligned} \frac{dy}{dx} &= F(y,x), \qquad y \in \mathbb{R}^p, \\ y(0) &= y_0. \end{aligned}$$

We rewrite this as a system of integral equations $\mathbf{G}(\mathbf{y}) = \mathbf{KF}(\mathbf{y})$ where $\mathbf{G}, \mathbf{F} \in \mathbb{R}^p$ are column vectors with i-th components G_i and F_i respectively. As before $\mathbf{K}$ refers to the integration operator. Consider a discretized version of the integral equations and suppose that each component of the vectors g_j and f_j, i.e. the values of $\mathbf{G}$ and $\mathbf{F}$ at scale j, can be represented as

$$\begin{aligned} g_{j,i} &= \gamma_{0,j,i} + \gamma_{1,j,i}\delta_j^2, \\ f_{j,i} &= \theta_{0,j,i} + \theta_{1,j,i}\delta_j^2, \end{aligned}$$

where $i = 1, \ldots, p$ is the component of the vector.

At scale $j-1$ they can then be written as

$$\begin{aligned} g_{j-1,i} &= \gamma_{0,j-1,i} + \gamma_{1,j-1,i}\delta_{j-1}^2, \\ f_{j-1,i} &= \theta_{0,j-1,i} + \theta_{1,j-1,i}\delta_{j-1}^2. \end{aligned}$$

where the new γ- and θ-functions are given by a recursion relation similar to the scalar case. Letting $\mathbf{S}$ and $\mathbf{D}$ denote componentwise application of S and D, we have

$$\begin{aligned} \gamma_{0,j-1} &= \mathbf{S}\gamma_{0,j}, \\ \theta_{0,j-1} &= \mathbf{S}\theta_{0,j}, \\ \gamma_{1,j-1} &= \frac{1}{4}\mathbf{S}\gamma_{1,j} + \frac{1}{16}\mathbf{D}\theta_{0,j} + \frac{1}{16}(\mathbf{S}J_{\theta_{0,j}} + \mathbf{D}J_{\gamma_{0,j}})\bar{d}_{j-1} + \frac{1}{32}h_{\gamma_0}, \\ \theta_{1,j-1} &= \frac{1}{4}\mathbf{S}\theta_{1,j} + \frac{1}{16}(\mathbf{D}J_{\theta_{0,j}})\bar{d}_{j-1} + \frac{1}{32}h_{\theta_0}, \\ \bar{d}_{j-1} &= J_{\gamma_{0,j}}^{-1}(\mathbf{S}\theta_{0,j} - \mathbf{D}\gamma_{0,j}). \end{aligned} \tag{10}$$

The vectors h_{γ_0} and h_{θ_0} have components given by

$$h_{\gamma_0,i} = \bar{d}_{j-1}^T(\mathbf{S}H_{\gamma_{0,j,i}})\bar{d}_{j-1}, \qquad h_{\theta_0,i} = \bar{d}_{j-1}^T(\mathbf{S}H_{\theta_{0,j,i}})\bar{d}_{j-1}, \qquad i = 1, \ldots, p,$$

where $H_{\gamma_{0,j,i}}$ and $H_{\theta_{0,j,i}}$ are the Hessian matrices (the matrices of second derivatives with respect to the variables at scale j) of the i-th component of $\gamma_{0,j}$ and $\theta_{0,j}$ respectively. Similarly, $J_{\theta_{0,j}}$ and $J_{\gamma_{0,j}}$ are the Jacobian matrices of $\gamma_{0,j}$ and $\theta_{0,j}$ with respect to the variables at scale j.

At the coarsest scale $j = 0$ we now obtain a system of coupled non-linear algebraic equations which can be solved for the averages of the variables y_i.

The recursion relations above are exactly the multivariable analogs of the relations presented in the previous subsection for the single differential equation case.

3.2 Boundary value problems

To study steady states of reaction diffusion problems, we need to apply the procedure to boundary value problems (BVP), as opposed to the initial value problems above. Consider for example a second order differential equation on the unit interval with dirichlet boundary conditions,

$$\begin{aligned} u_{xx} &= F(u, u_x), \qquad\qquad x \in (0,1) \\ u(0) &= u_0, \\ u(1) &= u_1. \end{aligned}$$

Setting $y_1 = u$ and $y_2 = u_x$, we can rewrite this as the integral equations

$$\begin{aligned} y_1(x) &= u_0 + \int_0^x y_2(s)ds, \\ y_2(x) &= y_2(0) + \int_0^x F(y_1(s), y_2(s))ds. \end{aligned}$$

More generally, we consider equations of the form,

$$\begin{aligned} g_1(y_1(x), y_2(x)) &= y_1(0) + \int_0^x f_1(y_1(s), y_2(s), s)ds, \\ g_2(y_1(x), y_2(x)) &= y_2(0) + \int_0^x f_2(y_1(s), y_2(s), s)ds. \end{aligned}$$

When the reduction operation is performed all the way to the final scale, this results in an equation of the form

$$\begin{aligned} G_1(v, w) &= y_1(0) + F_1(v, w), \\ G_2(v, w) &= y_2(0) + F_2(v, w), \end{aligned}$$

where v and w are the averages of the variables y_1 and y_2 over the interval. The functions G_1 and G_2 are obtained by reducing the functions g_1 and g_2 all the way to the final scale (and similarly for F_1 and F_2). If the values of y_1 and

y_2 at $x = 0$ were given, then the above equations could be solved for v and w. If partial information is available at each boundary, as in the BVP case, the reduction procedure must be performed starting from each boundary [13]. We then consider the backward integral equations,

$$\begin{aligned} g_3(y_1(x), y_2(x)) &= y_1(1) + \int_1^x f_1(y_1(s), y_2(s), s)ds, \\ g_4(y_1(x), y_2(x)) &= y_2(1) + \int_1^x f_2(y_1(s), y_2(s), s)ds. \end{aligned}$$

The reduction of the above equations results in equations of the form

$$\begin{aligned} G_3(v, w) &= y_1(1) + F_3(v, w), \\ G_4(v, w) &= y_2(1) + F_4(v, w). \end{aligned}$$

These are also nonlinear algebraic equations in the variables v, w, the same averages of y_1, y_2 as above. Also, importantly, these incorporate the solution values at the right boundary, $x = 1$. The above four equations along with two boundary conditions can be solved for the averages of the solution. How to obtain the explicit form of the reduced equations are discussed in Section 4, in the context of our specific problem.

3.3 Block division

The reduction procedure can be carried out over the entire domain at once, or simultaneously over a collection of its parts. As indicated earlier, the reduction procedure in the nonlinear case involves truncating a Taylor series. As very coarse scales are reached, the Taylor series approximations can start causing inaccuracies, since the variable of expansion at any scale is the size of the interval $\delta_j = 2^{-j}$. A way around this problem is to divide the domain (which is scaled to the unit interval) into subdomains. If N subdomains are used, the size of the interval is then $2^{-j}/N$ at scale j. The reduction is performed till scale $j = 0$ *for each subdomain* is reached, resulting in nonlinear algebraic equations for the solution average on that subdomain, and the boundary values on that subdomain. Enforcing continuity between adjacent domains gives a closed system of equations that can be solved for the average of the solution over each subdomain.

For the example in the previous section, consider dividing the domain into two equal subdomains, which we label 1 and 2. Full forward reduction on the first domain results in nonlinear equations of the form

$$\begin{aligned} h_1(v^{(1)}, w^{(1)}) - y_1(0) &= 0, \\ h_2(v^{(1)}, w^{(1)}) - y_2(0) &= 0. \end{aligned}$$

Full reduction of the backward integral equation, results in

$$\begin{aligned} y_1(0.5) - h_3(v^{(1)}, w^{(1)}) &= 0, \\ y_2(0.5) - h_4(v^{(1)}, w^{(1)}) &= 0. \end{aligned}$$

For the second domain we similarly obtain

$$\begin{aligned} h_5(v^{(2)}, w^{(2)}) - y_1(0.5) &= 0, \\ h_6(v^{(2)}, w^{(2)}) - y_2(0.5) &= 0. \end{aligned}$$

and

$$\begin{aligned} y_1(1) - h_7(v^{(2)}, w^{(2)}) &= 0, \\ y_2(1) - h_8(v^{(2)}, w^{(2)}) &= 0. \end{aligned}$$

Eliminating $y_1(0.5)$ and $y_2(0.5)$ results in the set of equations

$$\begin{aligned} h_1(v^{(1)}, w^{(1)}) - y_1(0) &= 0, \\ h_2(v^{(1)}, w^{(1)}) - y_2(0) &= 0, \\ h_5(v^{(2)}, w^{(2)}) - h_3(v^{(1)}, w^{(1)}) &= 0, \\ h_6(v^{(2)}, w^{(2)}) - h_4(v^{(1)}, w^{(1)}) &= 0, \\ y_1(1) - h_7(v^{(2)}, w^{(2)}) &= 0, \\ y_2(1) - h_8(v^{(2)}, w^{(2)}) &= 0. \end{aligned}$$

supplemented by two boundary conditions, one at each boundary. This set of reduced equations can be solved for the remaining boundary values and the averages of the variables y_1 and y_2 on the two subdomains. For equal size blocks, as in this example, essentially the same final resulting equations would have have been obtained by performing a reduction on the entire domain till the scale $j = 1$ (but not exactly because of the Taylor series approximation). The procedure is, however, also applicable to blocks of different lengths. This last feature could be important in cases where the solution may vary relatively rapidly over certain parts of the domain, and slowly over others.

In summary, in this section, we have discussed the reduction procedure for a single non-linear equation in detail, and also described how this is extended to the multivariable case as well as the case of boundary-value problems. The implementation is described in the next section.

4 Reduced FitzHugh-Nagumo equations

The FitzHugh-Nagumo equations [12, 26] have been widely studied as a model of pattern formation in chemical and biological media. We are only concerned with steady states of these equations in one spatial dimension with no-flux boundary conditions. The equations model the concentration dynamics of two chemical species—an *activator* and an *inhibitor*. In the dimensioness form

$$\begin{aligned} u_t &= u - u^3 - v + u_{xx}, \\ v_t &= \delta v_{xx} + \epsilon(u - a_1(x)v - a_0(x)) \end{aligned}$$

u and v represent the (dimensionless) activator and inhibitor concentrations respectively; a_1 and a_0 are kinetic parameters which, in general, may vary in space; ϵ and δ (the dimensionless inhibitor diffusion coefficient) will be constant in our study.

Steady states of this system satisfy the elliptic equations

$$\begin{aligned} u_{xx} &= u^3 - u + v, \\ \delta v_{xx} &= \epsilon(a_1(x)v + a_0(x) - u), \end{aligned}$$

with no-flux boundary conditions.

We will consider separately the *non-diffusing inhibitor* case $\delta = 0$. In this case the variable v at steady state can be written in terms of u, and this results in the scalar elliptic equation

$$u_{xx} = u^3 + \alpha(x)u + \beta(x),$$

where $\alpha(x) = 1/a_1(x) - 1$ and $\beta(x) = -a_1(x)/a_0(x)$.

The first step in the implementation of the reduction procedure is to rewrite the equations as a set of first order differential equations. Thus, the given system can be written as

$$\begin{aligned} u_x &= w, \\ w_x &= u^3 + v - u, \\ v_x &= z, \\ z_x &= (-\epsilon/\delta)(u - a_1 v - a_0). \end{aligned}$$

These are supplemented by the no-flux boundary conditions

$$w(0) = z(0) = w(L) = z(L) = 0.$$

The differential equations are then written as integral equations,

$$\begin{aligned} u(x) - u(0) &= \int_0^x w(s)ds, \\ w(x) - w(0) &= \int_0^x (u^3(s) + v(s) - u(s))ds, \\ v(x) - v(0) &= \int_0^x z(s)ds, \\ z(x) - z(0) &= \int_0^x (-\epsilon/\delta)(u(s) - a_1(s)v(s) - a_0(s))ds, \end{aligned}$$

and discretized as in (5) at a sufficiently fine scale n. The discretization amounts to initializing the recursion relations as

$$\gamma_{0,n} = \begin{pmatrix} u_n \\ w_n \\ v_n \\ z_n \end{pmatrix}, \qquad \theta_{0,n} = \begin{pmatrix} w_n \\ u_n^3 + v_n - u_n \\ z_n \\ (-\epsilon/\delta)(u_n - a_{1,n}v_n - a_{0,n}) \end{pmatrix}.$$

Here $a_{1,n}, a_{0,n} \in \mathbb{R}^{2^n}$ are the discretizations at scale n of the functions $a_1(x)$ and $a_0(x)$; $\gamma_{1,n}$ and $\theta_{1,n}$ are set to zero.

In order to go from level to level we use the recursion relations in (10). Before we indicate the results of the reduction procedure, we make a couple of comments regarding the application of the S and D operators used in (10). Given a function $g_n(k, y_n(k))$ we need to evaluate $Sg_n(k, s_{n-1}(k), 0)$ and $Dg_n(k, s_{n-1}(k), 0)$ (as defined by (8)), where $s_{n-1} = S_{n-1}y_n$. In our case g_n will always be of the form $g_n(k, y_n(k)) = \alpha_n(k) f(y_n(k))$ for some $\alpha_n \in \mathbb{R}^{2^n}$ and function $f(y)$. In words, what this means is that the function g_n has an explicit spatial dependence through the function α in addition to the spatial dependence through the function f (whose argument is y_n). Then, by (8),

$$Sg_n(k, s_{n-1}(k), 0) = (S_{n-1}\alpha_n)(k) f(s_{n-1}(k)) =: \alpha_{n-1}(k) f(s_{n-1}(k))$$

and

$$Dg_n(k, s_{n-1}(k), 0) = (D_{n-1}\alpha_n)(k) f(s_{n-1}(k)).$$

Note, if α_n is constant, then $Dg_n \equiv 0$.

As an example, if $g_n = \alpha_n u_n^3$, then the application of the S and D operators result in $Sg_n = (S\alpha_n)u_{n-1}^3$ and $Dg_n = (D\alpha_n)u_{n-1}^3$. Thus, effectively what results is that the operators S and D are applied to the explicitly spatially depending part, and the argument of the function becomes the dependent variable at the next coarser scale.

We also note that in our case the interval is $[0, L]$ instead of $[0, 1]$ as before. This rescaling only affects the size of the subintervals, which are now $\delta_n = L2^{-n}$.

Using the multivariate recursion relations in (10), one obtains

$$\gamma_{0,n-1} = S\gamma_{0,n} = \begin{pmatrix} u_{n-1} \\ w_{n-1} \\ v_{n-1} \\ z_{n-1} \end{pmatrix}.$$

Similarly the other recursion relations read:

$$\theta_{0,n-1} = S\theta_{0,n} = \begin{pmatrix} w_{n-1} \\ u_{n-1}^3 + v_{n-1} - u_{n-1} \\ z_{n-1} \\ (-\epsilon/\delta)(u_{n-1} - a_{1,n-1}v_{n-1} - a_{0,n-1}) \end{pmatrix}.$$

Since $J_{\gamma_{0,n}} = I$, the identity, we have $\bar{d}_{n-1} = \mathbf{S}\theta_{0,n} = \theta_{0,n-1}$, and the expressions for the other terms are

$$\gamma_{1,n-1} = \frac{1}{16}\begin{pmatrix} u_{n-1}^3 + v_{n-1} - u_{n-1} \\ (3u_{n-1}^2 - 1)w_{n-1} + z_{n-1} \\ (-\epsilon/\delta)(u_{n-1} - a_{1,n-1}v_{n-1} - a_{0,n-1}) \\ (\epsilon/\delta)(-w_{n-1} + a_{1,n-1}z_{n-1} + (D_{n-1}a_{1,n})v_{n-1} + D_{n-1}a_{0,n}) \end{pmatrix},$$

$$\theta_{1,n-1} = \frac{1}{16}\begin{pmatrix} 0 \\ 3u_{n-1}w_{n-1}^2 \\ 0 \\ (\epsilon/\delta)(D_{n-1}a_{1,n})z_{n-1} \end{pmatrix}.$$

The above equations illustrate the dependence of the γ- and θ-functions at scale $n-1$ on the variables at that scale. Note that the form of θ_0, γ_0, θ_1 and γ_1 is preserved under recursion—only the coefficients of the various terms change. This is easily seen by repeating the recursion relations. The functions we obtain will retain their functional form at any scale.

At scale 0, the coarsest scale, the above functions are

$$\gamma_{0,0} = \begin{pmatrix} u_0 \\ w_0 \\ v_0 \\ z_0 \end{pmatrix}, \qquad \theta_{0,0} = \begin{pmatrix} w_0 \\ u_0^3 + v_0 - u_0 \\ z_0 \\ (-\epsilon/\delta)(u_0 - c_4 v_0 - c_5) \end{pmatrix},$$

$$\gamma_{1,0} = \begin{pmatrix} c_1(v_0 + u_0^3 - u_0) \\ c_1((3u_0^2 - 1)w_0 + z_0) \\ (-\epsilon/\delta)c_1(u_0 - c_4 v_0 - c_5) \\ (-\epsilon/\delta)(c_1 w_0 - c_1 c_4 z_0 - \frac{c_2}{L} v_0 - \frac{c_3}{L}) \end{pmatrix},$$

$$\theta_{1,0} = \begin{pmatrix} 0 \\ 3c_1 u_0 w_0^2 \\ 0 \\ (\epsilon/\delta)\frac{c_2}{L} z_0 \end{pmatrix}.$$

The various c parameters are constants, which may depend on the medium properties through the functions $a_0(x)$ and $a_1(x)$:

$$c_1 = \frac{1}{16} \sum_{p=0}^{n-1} \frac{1}{4^p}, \tag{11}$$

$$c_2 = \frac{1}{2^n} \sum_{k=0}^{2^n-1} \left(\frac{k+1/2}{2^n} - \frac{1}{2} \right) a_{1,n}(k), \qquad c_4 = \frac{1}{2^n} \sum_{k=0}^{2^n-1} a_{1,n}(k),$$

$$c_3 = \frac{1}{2^n} \sum_{k=0}^{2^n-1} \left(\frac{k+1/2}{2^n} - \frac{1}{2} \right) a_{0,n}(k), \qquad c_5 = \frac{1}{2^n} \sum_{k=0}^{2^n-1} a_{0,n}(k).$$

The advantage is that it is possible to explicitly determine these various coefficients in terms of the coefficients of the equation we started with (material properties). The reduced equations at the coarsest scale are easily obtained from above. Recalling that here $K_0 = \delta_0 = L$, they are

$$
\begin{aligned}
u_0 + L^2 c_1(u_0^3 + v_0 - u_0) - u(0) &= \frac{L}{2} w_0, \\
w_0 + L^2 c_1((3u_0^2 - 1)w_0 + z_0) - w_0 &= \\
&\quad \frac{L}{2}\Big[u_0^3 + v_0 - u_0 + 3L^2 c_1 u_0 w_0^2\Big], \\
v_0 - L^2 \frac{\epsilon}{\delta} c_1(u_0 - c_4 v_0 - c_5) - v(0) &= \frac{L}{2} z_0, \\
z_0 - L^2 \frac{\epsilon}{\delta}\left(c_1 w_0 - c_1 c_4 z_0 - \frac{c_2}{L} v_0 - \frac{c_3}{L}\right) - z(0) &= \\
&\quad -\frac{L}{2}\frac{\epsilon}{\delta}\Big[u_0 - c_4 v_0 - c_5 - L^2(\frac{c_2}{L} z_0)\Big].
\end{aligned} \tag{12}
$$

These equations contain the values of the variables at the left end of the domain in which they are being reduced (in this case $x = 0$).

The integral equations resulting from the backward integration are

$$
\begin{aligned}
u(L) - u(L-x) &= \int_0^x w(L-s)ds, \\
w(L) - w(L-x) &= \int_0^x (u^3(L-s) + v(L-s) - u(L-s))ds, \\
v(L) - v(L-x) &= \int_0^x z(L-s)ds, \\
z(L) - z(L-x) &= -\frac{\epsilon}{\delta}\int_0^x [u(L-s) - a_1(L-s)v(L-s) - a_0(L-s)]ds,
\end{aligned}
$$

and reduce to

$$
\begin{aligned}
u(L) - (u_0 + L^2 c_1(u_0^3 + v_0 - u_0)) &= \frac{L}{2} w_0, \\
w(L) - (w_0 + L^2 c_1((3u_0^2 - 1)w_0 + z_0)) &= \\
&\quad \frac{L}{2}\Big[u_0^3 + v_0 - u_0 + 3L^2 c_1 u_0 w_0^2\Big], \\
v(L) - (v_0 - L^2 \frac{\epsilon}{\delta} c_1(u_0 - c_4 v_0 - c_5)) &= \frac{L}{2} z_0, \\
z(L) - (z_0 - L^2 \frac{\epsilon}{\delta}(c_1 w_0 - c_1 c_4 z_0 - \frac{c_2}{L} v_0 - \frac{c_3}{L})) &= \\
&\quad -\frac{L}{2}\frac{\epsilon}{\delta}\Big[u_0 - c_4 v_0 - c_5 - L^2(\frac{c_2}{L} z_0)\Big].
\end{aligned} \tag{13}
$$

These reduced equations involve the values of the dependent variables on the right boundary ($x = L$). The overall set of reduced equations (12,13) should be supplemented with boundary conditions.

In summary, the reduction of the original differential equations results in non-linear algebraic equations for the averages of the solution variables, and their values at the endpoints. Division into blocks (as in Section 3.3) can be performed for these equations too. It is worth noting that the form of the equations in each block remains the same—only the coefficients differ.

The properties of the medium are embedded in the various coefficients calculated above. These coefficients can be analyzed in the limit as $n \to \infty$ (n is the starting scale for the reduction):

$$c_1 \to \frac{1}{12}$$

and the remaining constants tend to the first moments of the material coefficients,

$$\begin{aligned} c_2 &\to \int_0^1 (x - 1/2) a_1(Lx) dx, & c_4 &\to \int_0^1 a_1(Lx) dx, \\ c_3 &\to \int_0^1 (x - 1/2) a_0(Lx) dx, & c_5 &\to \int_0^1 a_0(Lx) dx. \end{aligned}$$

These constants depend neither on the parameters δ and ϵ (which are present explicitly in the reduced equations) nor on the boundary conditions. Also, when the coefficient functions are on the form $a_0(x/L)$ and $a_1(x/L)$, the constants are independent of L. The fact that the parameters in the reduced equations are present explicitly facilitates parametric/sensitivity analysis, and in our studies below we typically need to compute them only once. When the amplitude or the wavelength of the heterogeneity variation are varied, as in some of the cases we consider, the constants need to be recomputed though.

4.1 Non-diffusing inhibitor system

In the non-diffusing inhibitor case we obtain a pair of first order differential equations, by setting $w = du/dx$. After the reduction process, the equations read (see also [13, 15])

$$\begin{aligned} u_0 + L^2 c_1 (u_0^3 + c_4 u_0 + c_5) - u(0) &= \frac{L}{2} w_0, \\ w_0 + L^2 (\frac{c_2}{L} u_0 + c_1 c_4 w_0 + \frac{c_3}{L} + 3 c_1 u_0^2 w_0) - w(0) &= \\ \frac{L}{2} \Big[u_0^3 + c_4 u_0 + c_5 + L^2 (3 c_1 u_0 w_0^2 &+ \frac{c_2}{L} w_0) \Big], \\ u(L) - (u_0 + L^2 c_1 (u_0^3 + c_4 u_0 + c_5)) &= \frac{L}{2} w_0, \\ w(L) - (w_0 + L^2 (\frac{c_2}{L} u_0 + c_1 c_4 w_0 + \frac{c_3}{L} + 3 c_1 u_0^2 w_0)) &= \\ \frac{L}{2} \Big[u_0^3 + c_4 u_0 + c_5 + L^2 (3 c_1 u_0 w_0^2 &+ \frac{c_2}{L} w_0) \Big] \end{aligned}$$

The coefficient c_1 in these equations is the same as in (11). The remaining coefficients are

$$c_2 = \frac{1}{2^n}\sum_{k=0}^{2^n-1}\left(\frac{k+1/2}{2^n}-\frac{1}{2}\right)\alpha_n(k), \qquad c_4 = \frac{1}{2^n}\sum_{k=0}^{2^n-1}\alpha_n(k),$$
$$c_3 = \frac{1}{2^n}\sum_{k=0}^{2^n-1}\left(\frac{k+1/2}{2^n}-\frac{1}{2}\right)\beta_n(k), \qquad c_5 = \frac{1}{2^n}\sum_{k=0}^{2^n-1}\beta_n(k),$$

and

$$c_2 \to \int_0^1 (x-1/2)\alpha(Lx)dx, \qquad c_4 \to \int_0^1 \alpha(Lx)dx,$$
$$c_3 \to \int_0^1 (x-1/2)\beta(Lx)dx, \qquad c_5 \to \int_0^1 \beta(Lx)dx,$$

when $n \to \infty$. As before these are obtained by iterating the recursion relations till the coarsest scale ($j = 0$). These equations were first obtained in [13]. (Note that there is one difference between our equations and those obtained here, embodied in the coefficient c_2).

5 Results

Preliminary computations have been performed for the non-diffusing inhibitor version of the FitzHugh-Nagumo equations in [13, 15]. Averages of some steady state solution profiles over the entire domain were obtained there using the reduction methods. The results—for solution profiles which exhibited small amplitude variations around a spatially uniform solution—compared favorably with those from converged discretizations of the PDE.

We analyze here both the non-diffusing and the diffusing inhibitor cases, and perform the reduction operations over "blocks", so that we can deal with solutions exhibiting higher amplitude spatial variations, such as front- and pulse-like solutions. The blocks are then pieced together to obtain reduced equations for the entire domain as in Section 3.3 above. Such a procedure still results in a significant reduction in the number of equations which need to be solved. We will focus on the faithfulness of the reduced equations in capturing the detailed static bifurcation behavior with respect to both system parameters and "heterogeneity" parameters, such as the amplitude and wavelength of spatial variations of the medium. Since the algebraic equations we solve do not, in general, constitute the right hand side of a dynamical system, we do not expect non-static bifurcations (like Hopf bifurcations) to be faithfully captured.

5.1 Non-diffusing inhibitor system

The equations, with no-flux boundary conditions clearly admit several uniform steady states; in addition, steady states like fronts and pulses are admitted.

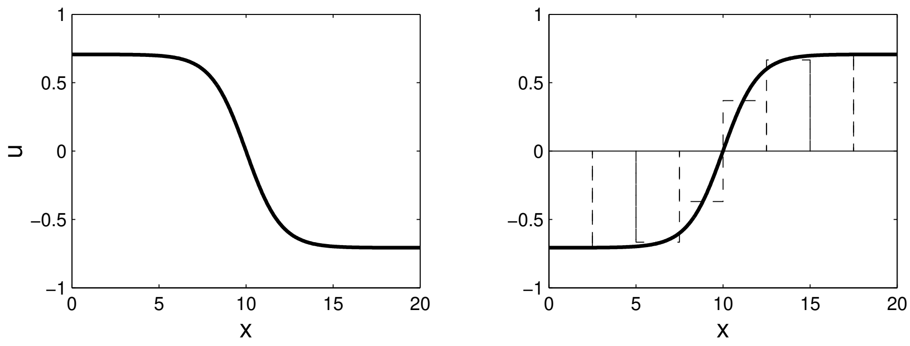

Figure 1: Two antisymmetric stationary front profiles for the homogeneous FHN equation with non-diffusing inhibitor: $L = 20$, $\alpha = 0.5$, $\beta = 0$. Dashed line shows the corresponding coarse profile.

These are some of the simplest coherent structures that can be regarded as building blocks for more complex patterns.

We focus on the case $\beta = 0$. In this case, static fronts exist in the infinite domain (and hence in a finite domain we expect static fronts at and near $\beta = 0$). The infinite-domain fronts possess a reflection symmetry: $x \to L - x, u \to -u$.

Figure 1 shows such a front at a particular parameter set $L = 20, \alpha = 0.5$; reflecting this front about the centerline (i.e. replacing x by $L - x$) is also a stationary solution. We look for these fronts in the reduced equations (using 8 blocks) and successfully captures their coarse features (dashed line in Figure 1). The average of the solution over a part of the domain, for example $[0, L/8]$, is well captured (compared to a converged finite difference solution) by the 8-block reduced equation (see below). Using a higher number of blocks will improve this agreement.

We explore the change of the solution as the domain size is decreased. This is equivalent to studying the effect of increasing the diffusion coefficient of the activator, starting from $D = 1$. The front solution gradually becomes less steep; the upper part of the front decreases in height and the lower part of the front decreases in depth. Eventually we find that a pitchfork bifurcation occurs at $L = 4.444$. At this parameter value the "front" solution becomes completely flat, and the branch of fronts meets the branch of steady states $u = 0$, and connects via a pitchfork bifurcation (see Figure 2).

For reduced equations with an even number of equally spaced blocks (for example 8), the reflection property of the full equations is preserved. Performing their bifurcation analysis we again find a pitchfork bifurcation; the location of the bifurcation point in the reduced system agrees with the actual bifurcation point to three decimal places. Reduced and full equation bifurcation diagrams are shown in Figure 3.

We now consider a *heterogeneous* version of the FHN equations, keeping $\beta \equiv 0$ and using $\alpha(x) = 0.5 + 0.2\cos(8\pi x/L)$. Heterogeneous versions of FHN

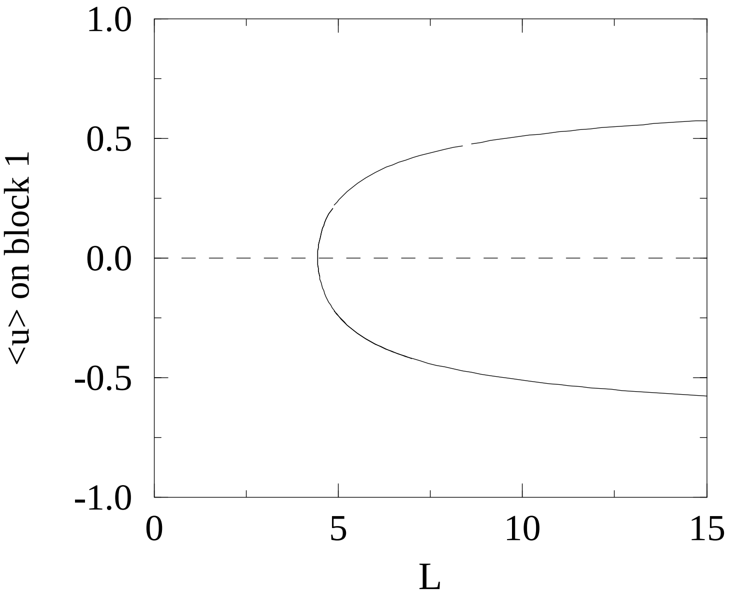

Figure 2: Bifurcation diagram of stationary fronts in the FHN equation with non-diffusing inhibitor, $\alpha = 0.5$, $\beta = 0$, showing the presence of a pitchfork bifurcation. The dashed line is the branch of homogeneous solutions $u = 0$.

equations are used to model reactions in distributed media with spatially varying kinetics (e.g. composite catalysts). We consider a periodic, antisymmetric (under $x \to L - x$) heterogeneity with four wavelengths over the computational domain.

The steady states of these heterogeneous FHN equations are spatially modulated fronts. A typical solution profile is shown in Figure 4, where the effect of the heterogeneity and antisymmetry is clearly seen. The coarse profile given by the reduced equations is indicated with dashed lines. Just as in the homogeneous case, the reduced equations capture the averages of the full solution over parts of the domain successfully (see below).

As the computational domain shrinks (keeping four heterogeneity wavelengths) we again find a pitchfork bifurcation involving the wavy front, its symmetric counterpart and the flat solution. The bifurcation point occurs again at $L = 4.444$. This is seen in Figure 5 where the solid line shows the bifurcation diagram obtained from the full system and the dots represent the results from the reduced equations.

Since in all these cases, the coefficients for the reduced equations are computed "off-line", the time taken to solve these reduced equations computationally, is basically determined by the size of the reduced equation. The converged computation for the steady state of the reduced equation at a particular parameter value only takes a few seconds on a Silicon graphics work station.

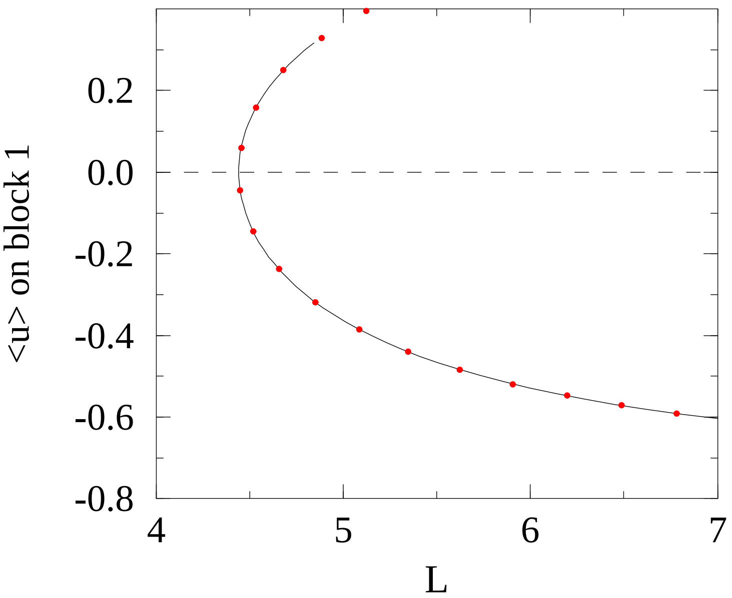

Figure 3: Pitchfork bifurcation of stationary fronts in the homogeneous FHN equation with non-diffusing inhibitor: solid line indicate results from a finite-difference discretization of the full system; dots indicate the results from the reduction procedure using $n_b = 8$, leading to $2n_b + 2 = 18$ eqns. The blocks are of equal width.

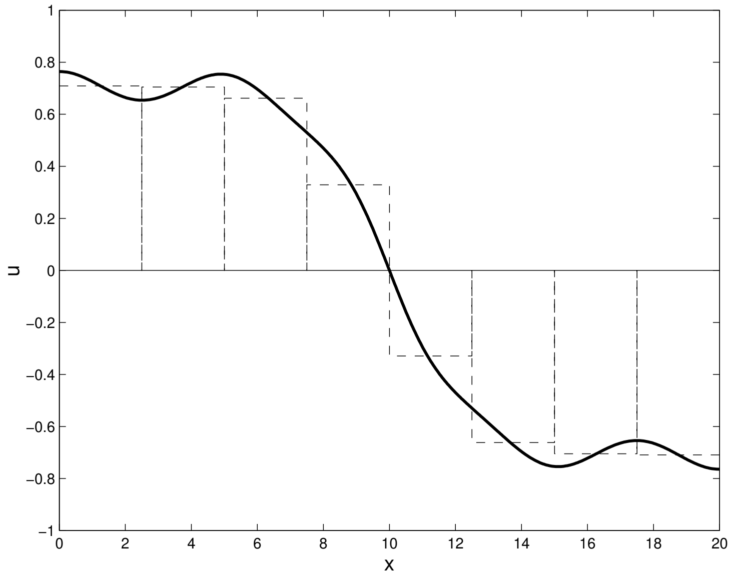

Figure 4: Stationary front profile for the heterogeneous FHN equations with non-diffusing inhibitor: $\alpha(x) = 0.5 + 0.2\cos(8\pi x/L)$, $\beta \equiv 0$ and $L = 20$. Dashed line shows the corresponding coarse profile.

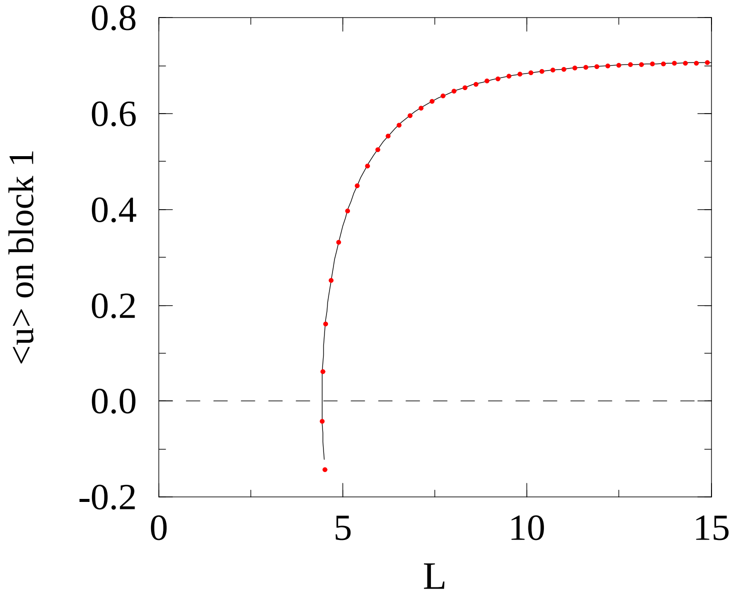

Figure 5: Bifurcation diagram of stationary fronts in the heterogeneous FHN equation with non-diffusing inhibitor.

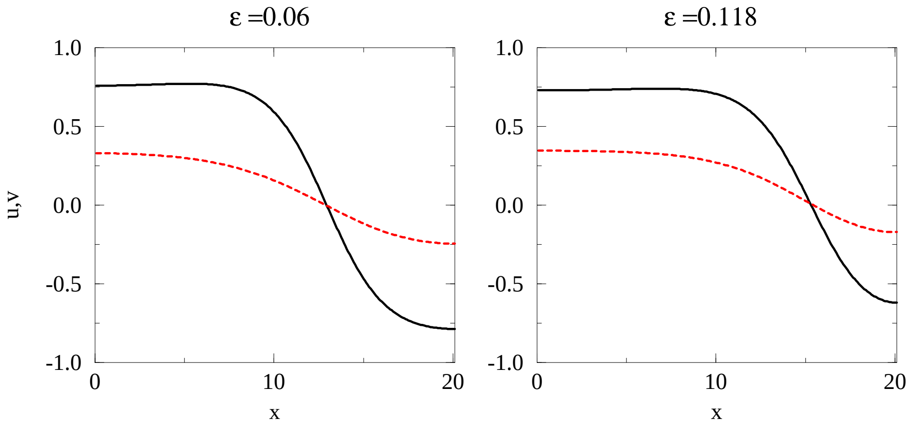

Figure 6: Front profiles of u (solid) and v (dashed) far before ($\epsilon = 0.06$) and just after ($\epsilon = 0.118$) the turning point. Parameters are $a_1 = 2$, $a_0 = 0.03$, $\delta = 0.5$.

5.2 Diffusing inhibitor system

Beyond modeling pattern formation in chemical and biological systems, the diffusing inhibitor FHN equations (with no flux BC for both species) have been recently studied in the context of distributed control [31]. In this case too, we shall be concerned with front-like solutions. Figure 6(a) shows one such front profile. These fronts are no longer invariant to antisymmetry about the middle of the domain: the steepest part of the front is now located closer to the right-hand boundary of the domain.

We will investigate the behaviour of this solution, as we vary the parameter ϵ, keeping the other parameters fixed: $\delta = 0.5$, $a_0 = 2.0$, $a_1 = 0.03$ and $L = 20$. Increasing ϵ this branch of stationary fronts turns around at $\epsilon = 0.118$ (compare with the results in [31]). The bifurcation diagram is shown in Figure 7. As one moves along the branch, the location of the "front" changes—it moves towards the right boundary for increasing ϵ. Figure 6(b) shows a front just beyond the saddle-node bifurcation.

For the reduced problem the domain was again broken up into $n_b = 8$ subdomains of equal sizes, leading to a total of $4n_b + 4 = 36$ equations. The reduced bifurcation diagram is shown in Figure 7, overlaid on the detailed bifurcation diagram; clearly the behaviour of the fronts of the full system is accurately captured. This happens even though the location of the relatively steep variation of the front is changing as a function of parameters, while the division of the domain into subdomains is unchanged.

This computation was repeated in the case of heterogeneous kinetics: $a_1(x) = 2.0 + 0.4\cos(8\pi x/L)$. As seen in Figure 8, the front profile reflects the underlying heterogeneity. The branch of fronts (solid line in Figure 9) possesses a turning point. The reduced equations (broken line/dots) are again clearly able to capture the heterogeneous front branch features.

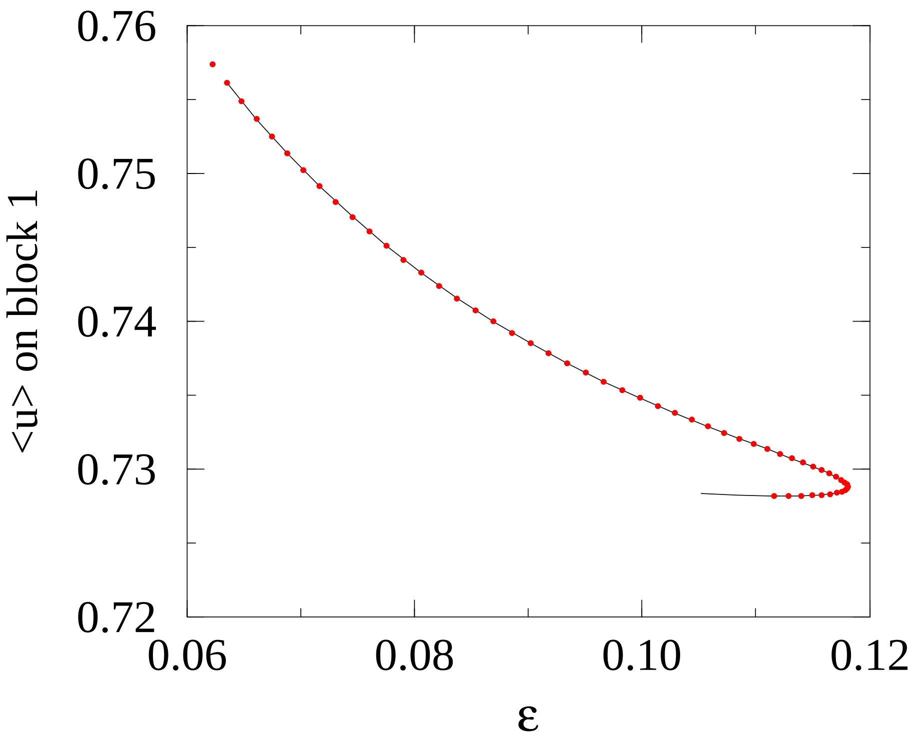

Figure 7: Bifurcation diagram of stationary fronts in the FHN equations with diffusing inhibitor: solid line indicates results from a finite-difference discretization of the full system; dots indicate results from the reduction procedure. Parameters are $a_1 = 2.0$, $a_0 = 0.03$, $L = 20$, $\delta = 0.5$. The reduction was performed with $n_b = 8$ blocks resulting in $4n_b + 4 = 36$ eqns.

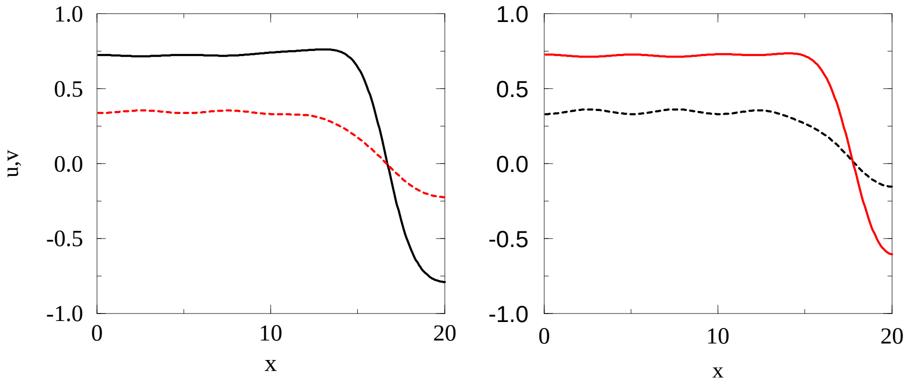

Figure 8: Front profiles of u (solid) and v (dashed) in the heterogeneous case $a_1(x) = 2.0 + 0.4\cos(8\pi x/L)$, $L = 20$ with $\epsilon = 0.06$ (left) and at the bifurcation point, $\epsilon = 0.1248$ (right).

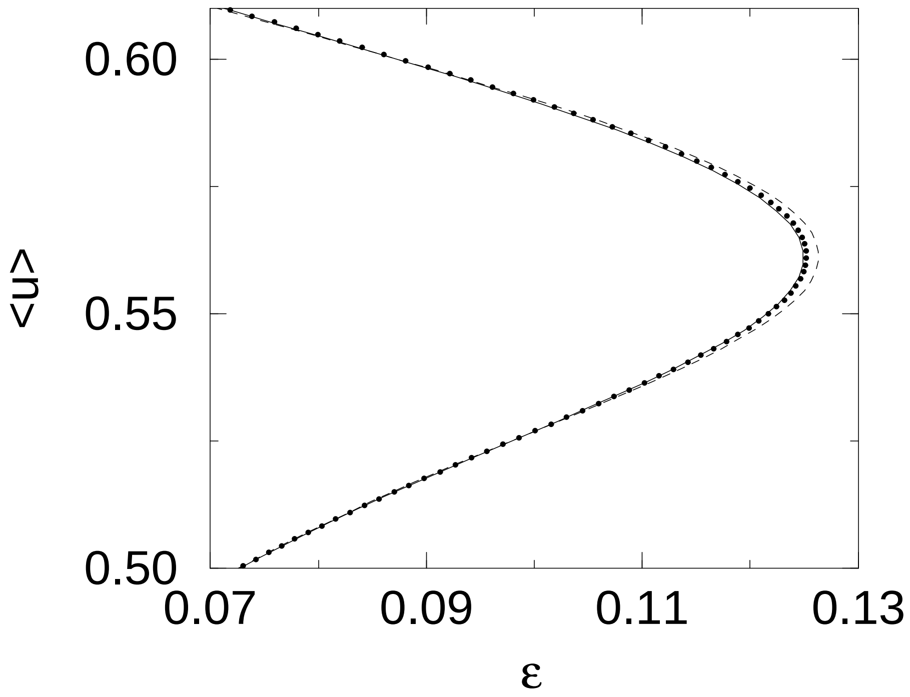

Figure 9: Bifurcation diagram of stationary fronts in heterogeneous FHN equation with diffusing inhibitor: solid line indicates results from a finite-difference discretization of the full system; dots and dashed line indicate results from the reduction procedure. Parameters are $a_0 = 0.03$, $L = 20$, $\delta = 0.5$. The heterogeneity is given by $a_1(x) = 2.0 + 0.4\cos(8\pi x/L)$. The reduction was performed with $n_b = 8$ (dashed line) and $n_b = 16$ (dots) blocks

n_b	$q(n_b)$	$m(n_b)$
8	0.3687506611360337	
16	0.3604152601388380	3.51
32	0.3596817294504204	3.93
64	0.3596335202496911	3.98

Table 1: Convergence for the homogeneous case; $q(n_b)$ is the average of the solution in the subdomain $[3L/8, L/2]$ using n_b blocks.

5.3 Convergence

We documented above the ability of the reduced equations to faithfully capture solution branch features of the detailed problem. We now discuss the rate of convergence of the reduced scheme as the block size approaches zero. In Figure 9 we see that increasing the number of blocks causes the reduced equation solution to approach the full solution branch.

To obtain the asymptotic rate of convergence, we select a measure of the solution q (e.g. the average of the solution profile over a subdomain) and explore its dependence on n_b, the total number of blocks used in the discretization. Assuming that the quantity of interest behaves like

$$q(n_b) = q(\infty) + c n_b^{-m} + \mathrm{o}\left(n_b^{-m}\right),$$

the asymptotic rate of convergence, m, is obtained by doubling n_b,

$$m(n_b) := \log_2 \left| \frac{q(n_b/4) - q(n_b/2)}{q(n_b/2) - q(n_b)} \right| \approx m, \qquad n_b \to \infty.$$

In all our experiments, c coefficients were computed with sufficiently high accuracy so as not to dominate the error at high block numbers. We find that the reduction scheme is asymptotically fourth order as $n_b \to \infty$. This is illustrated for the homogeneous case, in the non-diffusing FHN equations, for the front profile shown in Figure 1(a). The variation of the average of the solution in the subdomain $[3L/8, L/2]$ (the most quickly spatially varying part of the front) observed by doubling the number of blocks is shown in Table 1. Similar tests were also performed in the heterogeneous case. The corresponding results are shown Table 2. They are also suggestive of fourth order convergence. Final confirmation of the scheme order is obtained by comparing the difference of the reduced solution (in L_2 and the L_∞) from a sufficiently discretized one in Table 3. It is worth pointing out that such a comparison has to be made with the appropriate projection of the true solution on the same wavelet basis set (here piecewise constant functions) as the reduced solution. The analogue of the above table for the heterogeneous case is Table 4. Again the same observations made for the homogeneous case are valid here.

We now proceed to study bifurcations with respect to the heterogeneity parameters themselves; in particular, we study a saddle node bifurcation brought about as a result of increasing the amplitude of the heterogeneity in the diffusing

n_b	$q(n_b)$	$m(n_b)$
8	0.3290924019073874	
16	0.3192244683647248	
32	0.3183318538170801	3.47
64	0.3182730103708515	3.92
128	0.3182692738788159	3.98

Table 2: Convergence for the heterogeneous case; $q(n_b)$ is the average of the solution in the subdomain $[3L/8, L/2]$ using n_b blocks.

n_b	L_2 norm	$m(n_b)$	L_∞ norm	$m(n_b)$
8	4.573E-3		9.121E-3	
16	3.951E-4	3.53	8.225E-4	3.47
32	2.746E-5	3.85	7.504E-5	3.45
64	1.832E-6	3.91	4.978E-6	3.91

Table 3: Norm convergence for the homogeneous case.

n_b	L_2 norm	$m(n_b)$	L_∞ norm	$m(n_b)$
8	5.425E-3		1.082E-2	
16	4.973E-4	3.45	9.839E-4	3.46
32	3.339E-5	3.88	8.677E-5	3.50
64	2.109E-6	4.01	5.210E-6	4.05

Table 4: Norm convergence for the heterogeneous case.

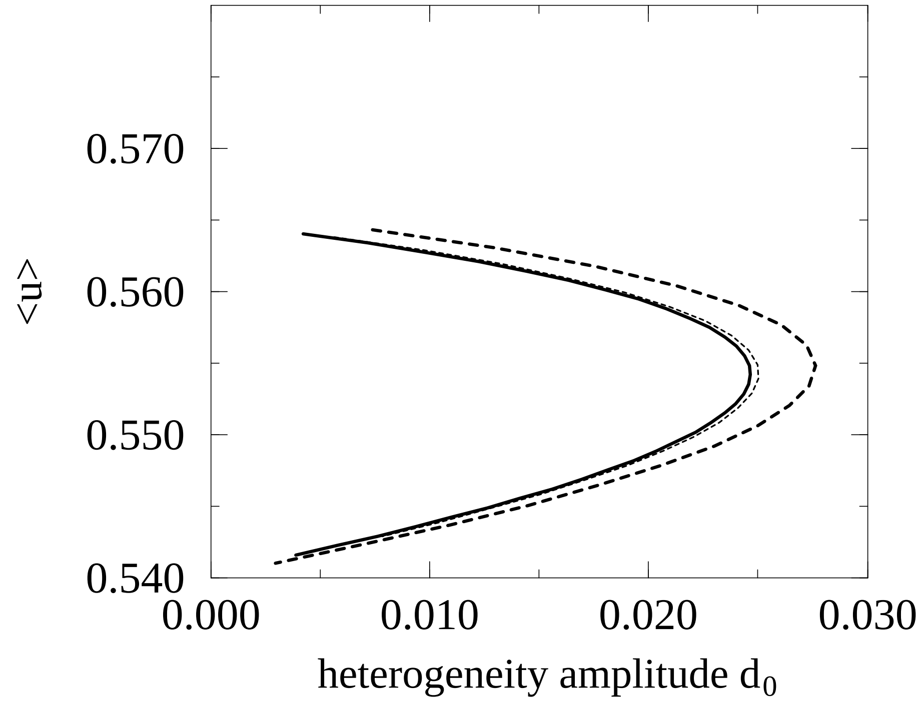

Figure 10: A saddle-node bifurcation occuring in the heterogeneous diffusing inhibitor FHN equation as the heterogeneity amplitude is increased. The parameters are $a_1 = 2$, $\epsilon = 0.1155$, $\delta = 0.5$, $L = 20$; $a_0(x) = 0.03 - d_0 \cos(8\pi x/L)$ where d_0 is the heterogeneity amplitude. Shown in the figure is the result obtained from finite-differences (dark solid line) and from the reduced equations: $n_b = 16$ (dark dashed line) and $n_b = 32$ (dashed line).

inhibitor FHN equations. The parameters are kept fixed at $L = 20$, $a_1 = 2$, $\delta = 0.5$, $\epsilon = 0.1155$. The coefficient a_0 varies in space as $a_0 = 0.03 - d_0 \cos(8\pi x/L)$. We consider the effect of increasing the coefficient d_0 starting from zero. We find in Figure 10 that as d_0 is increased starting from zero, a saddle node bifurcation occurs at $d_0 = 0.02466$. At that point the amplitude of the heterogeneity d_0 is comparable to the average value of the coefficient a_0. Also shown in the figure are the results obtained from the reduced equations for $n_b = 16$ and $n_b = 32$. Faithfulness in capturing the solution persists, but a greater number of blocks is needed than before to achieve comparable accuracy. Table 5 shows the variation of the reduced equation bifurcation point as a function of number of blocks.

We finally explore the effect of varying the heterogeneity wavelength, keeping its amplitude and all other system parameters fixed: $L = 20$, $\beta = 0$. The number of blocks in the reduced equations remains $n_b = 8$, and we consider a heterogeneity of the form $\alpha(x) = 0.5 + 0.2 \cos(2\pi kx/L)$. Taking $k = 0, 2, 4, ...$ we retain an even number of heterogeneity wavelengths in the computational

n_b	Bif. pt	$m(n_b)$
8	0.0542	
16	0.0276	
32	0.0250	3.35
64	0.02485	4.12

Table 5: Bifurcation point as a function of number of blocks n_b.

doman. The L_2 norm of the error between the reduced equation solution, and the appropriately projected full equation solution is shown in Figure 11.

The error remains small except when $k \approx n_b$, at which point the block size and the heterogeneity wavelength "resonate". This phenomenon has been observed in other reduction methods, see for example [17]. The reduced equations do in fact approach the "correct" limit as k becomes large. If in the above investigation a standard finite difference scheme (with fixed number of grid-points) were used, the problem would not be resolved and the error would typically grow as the parameter k increases.

6 Conclusions

In this paper, we analyzed the wavelet-based reduction procedure first presented in [13, 7] in the context of nonlinear reaction-diffusion equations. Preliminary work [13, 15] was concerned with steady states of the non-diffusing inhibitor FHN equations, which were characterized by relatively small amplitude variations (induced by heterogeneity) about a spatially uniform profile. The block reduction procedure suggested here allows the computation of solutions with large amplitude spatial variations, like pulses and fronts. From the point of view of pattern-formation, these are structures in the strongly non-linear regime.

We focused on the faithfulness of the reduced scheme in reproducing the spatially nonuniform solutions (in particular, fronts) and their bifurcations in both the non-diffusing and the diffusing inhibitor cases. Full reduction (to level zero) may not accurately capture these features and so an appropriate number of blocks must be retained. Nevertheless, the number of equations to be solved is still much less than the full discretization of the original system.

Static bifurcations (turning points, pitchforks) were accurately captured in both the homogeneous and heterogeneous medium cases. The reduction behaves asymptotically—when the individual block size approaches zero—as a fourth order scheme in both cases, and does converge to the appropriately projected true solutions. We observe that the reduced equations still capture the correct behavior when the heterogeneity scale becomes much smaller than the block sizes.

The conclusion is that such wavelet-based reduction techniques provide an attractive reduction alternative in problems where intense spatial variations of medium properties and system non-linearity play important roles.

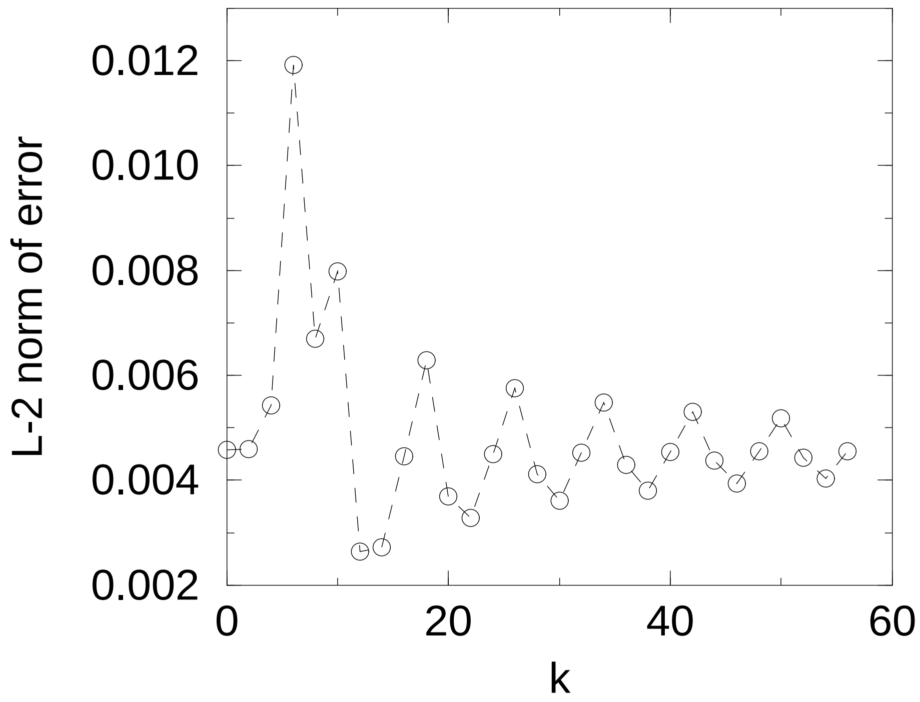

Figure 11: Effect of heterogeneity wavelength on the reduction process. Plotted is the L_2 norm of the error between the appropriately projected detailed solution and the solution of the reduced equations versus k, the number of heterogeneity wavelengths, for the non-diffusing FHN equations. Here $L = 20$, $\alpha(x) = 0.5 + 0.2\cos(2\pi kx/L)$, $\beta = 0$. The entry for $k = 0$ is the homogeneous case $\alpha \equiv 0.5$.

Acknowledgements. This work was partially supported by the National Science Foundation (through the KDI grant DMS-9872890) and a Humboldt Forschungspreis to I.G.K. Extensive discussions with Dr. A. Gilbert (now at AT&T), on whose Thesis this work is based, as well as with Profs. I. Daubechies and B. Engquist are gratefully acknowledged.

A Wavelets

We give here a brief introduction to wavelets and multiresolution analysis. More details can be found, for instance, in the book [9].

For our purposes, we can regard the wavelet basis, as a convenient set of basis functions, in which functions can be expanded, just like the Fourier basis. A distinguishing property of the wavelet basis is that it is built up of translates and dilates of a particular function.

A general framework for understanding wavelets and wavelet bases, is provided by a multiresolution analysis (MRA). An orthogonal MRA is made up of a ladder of nested closed function spaces,

$$\ldots \subset V_j \subset V_{j+1} \subset \ldots,$$

satisfying

$$\overline{\bigcup_{j\in\mathbb{Z}} V_j} = L_2(\mathbb{R}), \qquad \bigcap_{j\in\mathbb{Z}} V_j = \{0\}.$$

Moreover, the spaces V_j represent different level of coarseness (scale) in the sense that

$$f(x) \in V_j \quad \Leftrightarrow \quad f(2^{-j}x) \in V_0.$$

The zero space should also be invariant under integer translations,

$$f(x) \in V_0 \quad \Rightarrow \quad f(x-k) \in V_0, \qquad \forall k \in \mathbb{Z},$$

and there should exist a *scaling function*, $\phi \in V_0$, such that

$$\{\phi(x-k) : \ k \in \mathbb{Z}\},$$

is an L_2-orthonormal basis for V_0.

A number of important properties follows from the definitions above. Most importantly, the spaces V_j are spanned by dilates and translates of the scaling function. More precisely, the functions

$$\phi_{j,k}(x) = 2^{j/2}\phi(2^j x - k), \qquad k \in \mathbb{Z}. \tag{14}$$

form an L_2-orthonormal basis for V_j. The "differences" between successive V_j spaces have a similar structure: Let the orthogonal complement of V_j in V_{j+1} be denoted by W_j,

$$V_{j+1} = V_j \oplus W_j, \qquad V_j \perp W_j.$$

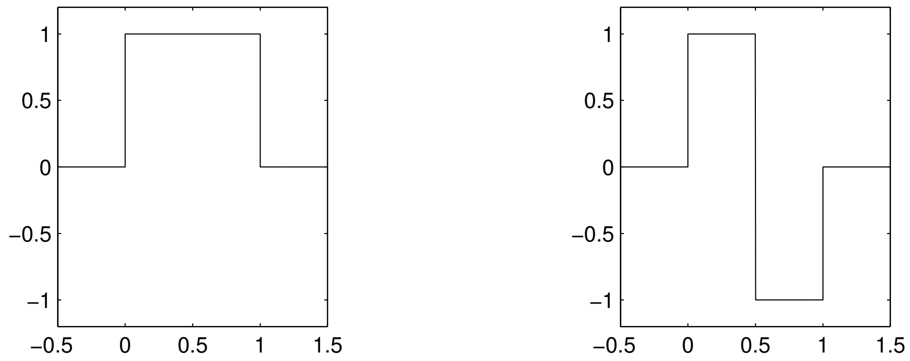

Figure 12: The scaling function $\phi(x)$ (left) and the wavelet function $\psi(x)$ (right) for the Haar basis.

The space V_j is the next coarser space with respect to V_{j+1} and W_j is the contrast space. Then, $L_2(\mathbb{R}) = \overline{\bigoplus_{j\in\mathbb{Z}} W_j}$ and there exists a *mother wavelet*, $\psi \in W_0$, with properties corresponding to that of ϕ; the functions

$$\psi_{j,k}(x) = 2^{j/2}\psi(2^j x - k), \qquad k \in \mathbb{Z}. \tag{15}$$

form an L_2-orthonormal basis for W_j. This mother wavelet can be constructed explicitly from a given MRA.

The simplest MRA is the one built on the Haar basis, where the scaling function and the mother wavelet are given by

$$\phi(x) = \begin{cases} 1, & \text{if } 0 \le x \le 1, \\ 0, & \text{otherwise,} \end{cases} \qquad \psi(x) = \begin{cases} 1, & \text{if } 0 \le x \le 1/2, \\ -1, & \text{if } 1/2 < x \le 1, \\ 0, & \text{otherwise.} \end{cases}$$

See Figure 12. This is the basis we use in this paper. We also restrict ourselves to the interval $[0, 1]$, meaning that the indices j and k above are limited to $j \ge 0$ and $k = 0, \dots, 2^j - 1$.

In the Haar case V_j contains piecewise constant functions. The coarsest level space V_0 represents functions that are constant over the entire interval. The other V_j spaces consist of functions which have successively finer structure, functions which are piecewise constant on 2^j intervals, each of length 2^{-j}. As the index j becomes large, the function space V_j will be able to approximate a continuous function well. Figure 13 shows a sample of functions at different scales which are successively coarser, ranging from $j = 3$ to $j = 0$.

We see that V_j can be thought of as arising out of V_{j+1} from an "averaging" over every adjacent pair of intervals. Thus, if we consider a function belonging to V_{j+1}, its projection ("component") on V_j is obtained as an arithmetic mean of every adjacent pair of intervals (there are half as many intervals as in V_{j+1}). On the other hand, its component in W_j is the function which contains the

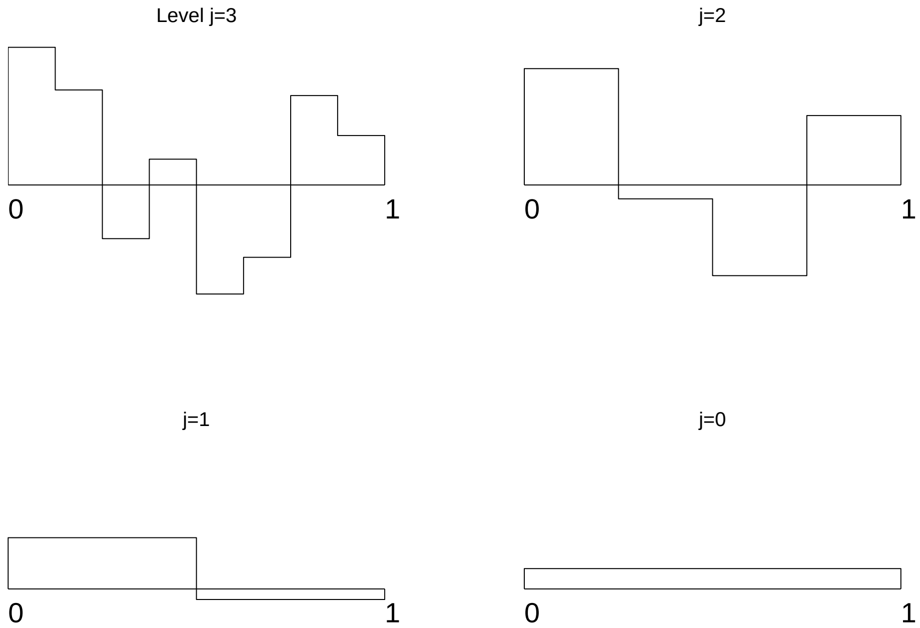

Figure 13: Sample functions at different (wavelet) scales: Successively coarser scales from $j = 3$ to $j = 0$

difference between the values at adjacent intervals. Thus, the decomposition of a function in the space V_{j+1} into a component in V_j and a component in W_j amounts to computing sums and differences of the function values at every pair of intervals.

B A bird's-eye view of the reduction procedure

In this section, we present a step-by-step picture of how the reduction procedure can be implemented for other problems. The specific details of the reduction procedure for two versions of the Fitzhugh-Nagumo equations are presented in the text. The starting point is the detailed equations, which are in the form of ordinary differential equations. These can further be written as a set of first order differential equations in a standard way.

1. Divide the domain into a suitable number of blocks.

2. Rewrite the set of first order differential equations as integral equations. These integral equations contain as parameters, the values of variables at boundaries of the domain (subdomains). When dealing with boundary value problems, it is necessary to write the integral equations that follows from starting at each end of the domain.

3. Discretize the equations. This results in equations of the form $G(y_n) = KF(y_n)$, where y_n is the dependent variable at the starting scale n, assumed to be large enough to adequately resolve features of the variations of the coefficients.

4. The reduction procedure for the above equations, is implemented in terms of recursion relations involving the functions γ_0, γ_1 (which are "pieces" of G) and θ_0 and θ_1 (which are pieces of F). Initialize the recursion so that $\gamma_{1,n} = \theta_{1,n} = 0$. The functions $\gamma_{0,n}$ and $\theta_{0,n}$ and their functional dependence on the dependent variable, as well as explicit dependence on the spatial variable (via spatially varying coefficients) are determined directly from the equation and thus known at this stage.

5. Perform one step of the recursion procedure involving these functions, using the relations described in the text (which are based on Taylor series approximations). This will determine the functional form of the functions $\gamma_{0,n-1}$, $\theta_{0,n-1}$, $\gamma_{1,n-1}$ and $\theta_{1,n-1}$ at scale $n-1$. This will also suggest the functional forms of these terms at lower scales (can be checked by doing a couple of recursions explicitly).

6. Implement this reduction step all the way until scale $n = 0$ in each block. The functional form of the reduced equations is determined from above. Note that all integral equations (both forward and backward) are reduced. Obtain the coefficients of the various terms at this lowest scale. This can often be done explicitly (as was done, for example, in the text). The form of the reduced equation is the same from block to block, but the coefficients differ.

7. Solve the reduced equations for the averages of the variables over each block as well as unknown boundary values (i.e. values at the boundary of the entire domain) of the variable. (The values of the variable at the boundaries of each block can be eliminated by manipulating the equations as suggested in the text.)

8. If parameteric sensitivity/bifurcation analysis is desired, it can be done directly on the reduced equations. The parameters are present in a transparent form in the reduced equations. In the case where the parameter affects the coefficients of the reduced equations (as for example the case when the amplitude of variation of a certain coefficient is a parameter), this has to be directly incorporated in the sensitivity analysis.

References

[1] U. Andersson, B. Engquist, G. Ledfelt, and O. Runborg. A contribution to wavelet-based subgrid modeling. *Appl. Comput. Harmon. Anal.*, 7:151–164, 1999.

[2] I. Babuška, G. Caloz, and J. E. Osborn. Special finite element methods for a class of second order elliptic problems with rough coefficients. *SIAM J. Numer. Anal.*, 31(4):945–981, 1994.

[3] M. Bär, A. K. Bangia, I. G. Kevrekidis, G. Haas, H. H. Rotermund, and G. Ertl. Composite catalyst surfaces: Effect of inert and active heterogeneities on pattern formation. *J. Phys. Chem.*, 100:19106–19117, 1996.

[4] T. W. Bell, G. H. Nyland, J. J. dePablo, and M. D. Graham. Combined brownian dynamics and spectral simulation of the recovery of polymeric fluids after shear flow. *Macromolecules*, 30:1806–1812, 1997.

[5] A. Bensoussan, J.-L. Lions, and G. Papanicolau. *Asymptotic Analysis for Periodic Structures*. North-Holland Publ. Comp., The Netherlands, 1978.

[6] G. Beylkin and M. Brewster. A multiresolution strategy for numerical homogenization. *Appl. Comput. Harmon. Anal.*, 2:327–349, 1995.

[7] G. Beylkin, M. E. Brewster, and A. C. Gilbert. A multiresolution strategy for numerical homogenization of nonlinear ODEs. *Appl. Comput. Harmon. Anal.*, 5:450–486, 1998.

[8] G. Beylkin and N. Coult. A multiresolution strategy for reduction of elliptic PDEs and eigenvalue problems. *Appl. Comput. Harmon. Anal.*, 5:129–155, 1998.

[9] I. Daubechies. *Ten Lectures on Wavelets*. SIAM, 1991.

[10] M. Dorobantu and B. Engquist. Wavelet-based numerical homogenization. *SIAM J. Numer. Anal.*, 35(2):540–559, April 1998.

[11] B. Engquist and O. Runborg. Wavelet-based numerical homogenization with applications. In T. J. Barth, T. F. Chan, and R. Haimes, editors, *Multiscale and Multiresolution Methods: Theory and Applications*, volume 20 of *Lecture Notes in Computational Science and Engineering*, pages 97–148. Springer-Verlag, 2001.

[12] R. A. FitzHugh. Impulses and physiological states in theoretical models of nerve membran. *Biophys. J.*, 1:445–466, 1961.

[13] A. C. Gilbert. *Multiresolution homogenization schemes for differential equations and applications*. PhD thesis, Princeton University, 1997.

[14] A. C. Gilbert. A comparison of multiresolution and classical one-dimensional homogenization schemes. *Appl. Comput. Harmon. Anal.*, 5(1):1–35, 1998.

[15] A. C. Gilbert. Using MRA reduction methods to characterize steady-states of reaction-diffusion equations. Available at URL `http://www.research.att.com/~agilbert/papers.html`, 1998.

[16] M. D. Graham, I. G. Kevrekidis, K. Asakura, J. Lauterbach, K. Krischer, H.-H. Rotermund, and G. Ertl. Effects of boundaries on pattern formation: Catalytic oxidation of CO on platinum. *Science*, 264:80–82, 1994.

[17] T. Y. Hou and X.-H. Wu. A multiscale finite element method for elliptic problems in composite materials and porous media. *J. Comput. Phys.*, 134(1):169–189, 1997.

[18] T. Y. Hou, X.-H. Wu, and Z. Cai. Convergence of a multiscale finite element method for elliptic problems with rapidly oscillating coefficients. *Math. Comp.*, 68(227):913–943, 1999.

[19] T. J. R. Hughes, G. R. Feijóo, L. Mazzei, and J.-B. Quicy. The variational multiscale method – a paradigm for computational mechanics. *Comput. Methods Appl. Mech. Engrg.*, 166:3–24, 1998.

[20] J. Kevorkian and J. D. Cole. *Multiple scale and singular perturbation methods.* Springer-Verlag, New York, 1996.

[21] S. Knapek. Matrix-dependent multigrid-homogenization for diffusion problems. *SIAM J. Sci. Stat. Comp.*, 20(2):515–533, 1999.

[22] X. Li and I. G. Kevrekidis. Front initiation on microdesigned composite catalysts. *Chaos*, 12:190–203, 2002.

[23] A.-M. Matache and C. Schwab. Homogenization via p-FEM for problems with microstructure. *Appl. Numer. Math.*, 33:43–59, 2000.

[24] A. Mehrabi and M. Sahimi. Coarsening of heterogeneous media: Application of wavelets. *Phys. Rev. Lett.*, 79(22):4385–4388, 1997.

[25] J. D. Moulton, J. E. Dendy, Jr., and J. M. Hyman. The black box multigrid numerical homogenization algorithm. *J. Comput. Phys.*, 142(1):80–108, 1998.

[26] J. S. Nagumo, S. Arimoto, and S. Yoshizawa. An active pulse transmission line simulating nerve axon. *Proc. IREE*, 50:2061–2070, 1962.

[27] N. Neuss, W. Jäger, and G. Wittum. Homogenization and multigrid. *Computing*, 66(1):1–26, 2001.

[28] P.-O. Persson and O. Runborg. Simulation of a waveguide filter using wavelet-based numerical homogenization. *J. Comput. Phys.*, 166:361–382, 2001.

[29] O. Runborg, C. Theodoropoulos, and I. G. Kevrekidis. Effective bifurcation analysis: a time-stepper based approach. *Nonlinearity*, 15:491–511, 2002.

[30] M. Sahimi and A. Mehrabi. Percolation and flow in geological formations: Upscaling from microscopic to megascopic scales. *Phys. A*, 266:136–152, 1999.

[31] S. Shvartsman and I. G. Kevrekidis. Nonlinear model reduction for control of distributed systems: a computer- assisted study. *AIChE J.*, 44:1579–1595, 1998.

[32] B. Z. Steinberg, J. J. McCoy, and M. Mirotznik. A multiresolution approach to homogenization and effective modal analysis of complex boundary value problems. *SIAM J. Appl. Math.*, 60(3):939–966, 2000.